Autoionization of doubly excited Ne atoms into excited ionic states

James A. R. Samson, Y. Chung, and E. M. Lee
Behlen Laboratory of Physics, University of Nebraska, Lincoln, Nebraska 68588-0111
(Received 22 August 1991)

The relative photoionization cross sections for the production of the $2s^22p^4(^3P)3p(^4P^o)$ satellite state of neon has been measured from its threshold at 52.1–60.5 eV. The spectrum is dominated by resonance structure, which can be identified as autoionization of numerous doubly excited neutral states.

PACS number(s): 32.80.Dz, 32.80.Fb, 32.50.+d, 32.90.+a

INTRODUCTION

In the photoionization process the primary photoelectron can interact with the remaining electrons in an atom to produce an excited state of the resulting ion (a satellite state). This process can occur directly, producing a continuum satellite state, or indirectly by resonance absorption into doubly excited neutral states that subsequently autoionizes. In our earlier studies of He [1,2], and that of Lindle *et al.* [3], both processes were observed in the production of the $He^+(n=2)$ satellite state. More recently, autoionization of doubly excited neutral states has been shown to dominate the production of satellites in the rare gases [4–14].

In the present work we have studied autoionization into the $2s^22p^4(^3P)3p(^4P^o)$ satellite state of Ne^+. The numerous resonances observed could be identified as members of Rydberg series of doubly excited states. These included most of the states observed by Codling, Madden, and Ederer [15] and several new states. The production of satellites and doubly excited neutral states can occur only through electron correlation processes. However, little is known about the coupling between the electrons in doubly excited states and how that coupling influences the strength of autoionization into a particular satellite state. Calculations have been made by Wijesundera and Kelly [16,17] using many-body perturbation theory to calculate the photoionization cross sections with excitation for some Ar satellite states. Their cross sections for the $(^3P)4p(^2P)$ satellite show numerous resonances caused by the inclusion of a limited number of doubly excited configurations in their calculations, for example, the $3s^23p^4(^1D)ndn'p$ levels. However, in our study of the argon $(^3P)4p(^2P)$ satellite [10] other much stronger doubly excited states dominated the resonance structure. This difference between theory and experiment is presumably caused by the limited number of excited configurations that could be included in the calculations. Our present studies of the Ne $(^3P)3p(^4P^o)$ satellite show that the strongest resonances are produced by autoionization of the $(^3P)3p(^2P)n(d,s)$ doubly excited levels.

EXPERIMENT

To study a specific satellite state we monitor, as a function of the incident photon energy, the fluorescence γ' produced by that state as it deexcites to a lower level. This technique is extremely selective because the fluorescence produced by each satellite state differs from that of any other state. The energy-level diagrams for the direct transition

$$2s^22p^6(^1S)+\gamma \rightarrow 2s^22p^4(^3P)3p(^4P^o)+e \quad \hookrightarrow 3s(^4P)+\gamma' \qquad (1)$$

and indirect transition

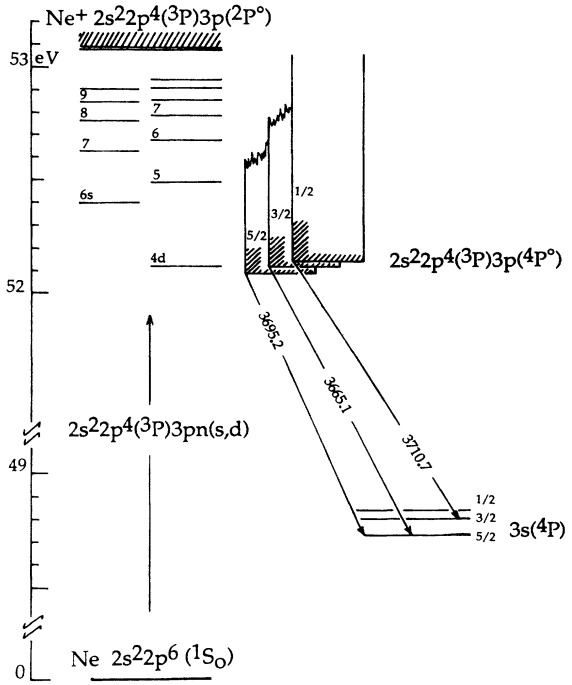

FIG. 1. Energy-level diagram of the $3p(^4P^o)$ satellite in relation to the doubly excited neutral states $(^3P)3pn(s,d)$. Autoinonization into the $3p(^4P^o)$ satellite is observed by monitoring the fluorescence produced as the satellite state subsequently decays into the $3s(^4P)$ level. the values of the fluorescent wavelengths shown are the vacuum wavelengths measured in angstroms.

$$2s^2 2p^6(^1S)+\gamma \rightarrow 2s^2 2p^4(^3P)3p(^2P^\circ)nl \hookrightarrow 3p(^4P^\circ)+e \rightarrow 3s(^4P)+\gamma'+e \quad (2)$$

are shown in Fig. 1. The $3p(^4P^\circ)$ satellite fluoresces between 3665 and 3778 Å as it decays to the $3s(^4P)$ state. However, by use of an interference filter centered on 3686 Å and with a bandpass of ±25 Å the observed fluorescence is restricted to the range between 3661 and 3711 Å, which allows transitions from each of the $^4P^\circ_{1/2,3/2,5/2}$ levels to be observed, as shown in Fig. 1.

The resulting energy dependence of the chosen satellite state, measured as a function of the incident photon energy, should be the same as that obtained by the use of photoelectron spectrometry. The advantage of the fluorescence technique is its inherent high-resolution capability, which is generally limited only by the resolution of the incident radiation. But in addition, two states with identical energies can be easily separated because they fluoresce with quite different wavelengths. This is true with the present choice of the $3p(^4P^\circ)$ satellite. This state lies within a few millivolts of the $(^1D)3s(^2D)$ satellite, which fluoresces at 406 Å. These two states have not been resolved by photoelectron spectrometry [13].

The experimental arrangement is shown in Fig. 2 and is similar to that used previously [10]. Radiation from the monochromator passed through a thin aluminum window separating the fluorescence chamber from the monochromator. Neon gas in the fluorescence chamber was maintained at a pressure of about 0.4 Torr. The incident radiation passed through a 51-mm-diam integrating sphere and was detected by a photomultiplier, which had been coated with sodium salicylate. The fluorescent radiation was detected at right angles to the path of the incident radiation by another photomultiplier. A quartz window was used as a vacuum seal and an interference filter was located in air between the window and the photomultiplier. Any fluorescent radiation that did not exit directly from the integrating sphere could make numerous collisions with the sphere's internal reflecting coating before finally escaping, because the reflectance of the coating was a uniform 98% between 4000 and 6000 Å.

Monochromatic radiation from the Undulator beam line at the Synchrotron Radiation Center in Stoughton, WI was used to excite the satellite state. A 6-m grazing incidence toroidal grating monochromator was used with a constant full width at half maximum bandpass of 0.13 Å. The equivalent energy resolution is 28 mV at threshold (52.1 eV).

The calibration of the monochromator wavelength scale was based on the known values of the $3p(^2P^\circ_{1/2,3/2})nd$ series limits [18,19], namely, 233.524 and 233.593 Å, respectively. An enlargment of this area is shown in Fig. 3. The data points occur in 0.02-Å steps. As the Rydberg series converge to the $2P^\circ_{1/2,3/2}$ limits the individual lines overlap, because of Doppler broadening, producing a true continuum. Thus we would expect two overlapping continua separated by 0.07 Å, the separation of the $^2P^\circ_{1/2,3/2}$ limits. Because the monochromator slit function is essentially triangular, a convolution with a step function will produce straight-line slopes as shown. The change in the $^2P^\circ_{3/2}$ slope halfway along is expected from the convolution. The onset of each slope for the $^2P^\circ_{1/2,3/2}$ steps will therefore occur 0.065 Å before the true thresholds. Thus the breaks in the curves occur at 233.46 and 233.53 Å as indicated in Fig. 3. Relying on the linearity of the monochromator drive, the wavelength scale is then calibrated. The estimated error is ±0.03 Å. To add confidence to this calibration we compare the positions of the $4d$ and $5d$ lines of the $3p(^2P^\circ)nd$ series shown in Fig. 4 with the values given by Codling, Madden, and Ederer [15]. The present work yields wavelengths of 237.90 and 236.26 Å, respectively, compared to 237.92 and 236.26 Å quoted by Codling, Madden, and Ederer.

The incident radiation was scanned, repetitively, from

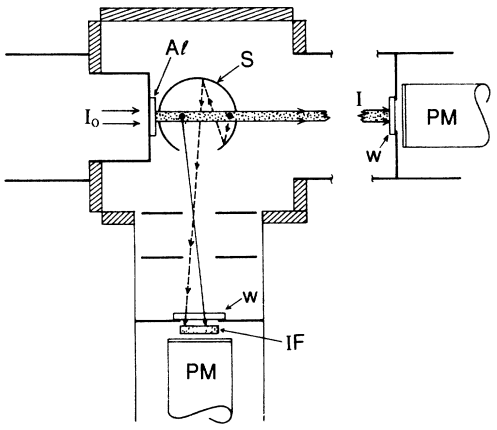

FIG. 2. Experimental arrangement showing the incident radiation I_0 entering the fluorescence chamber through a thin aluminum window (Al). Fluorescence radiation produced within the integrating sphere (S) is directed down to an interference filter (IF). The photomultipliers (PM) detect the radiation passing through the windows (W).

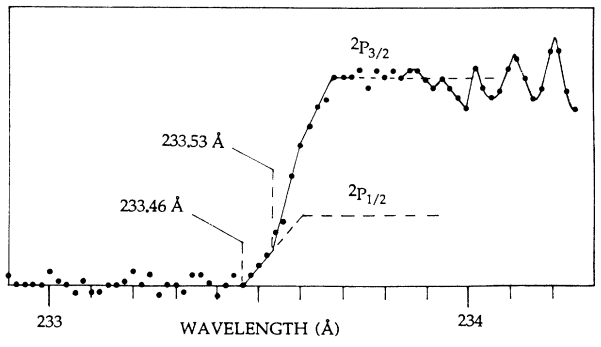

FIG. 3. Autoionization of the $3p(^2P)n(d,s)$ doubly excited series shown in the vicintiy of its series limit. Deconvolution of the limit allows an accurate calibration of the wavelength scale and indirectly shows the relative population of the $^2P_{3/2}$ and $^2P_{1/2}$ to be 2:1, in accordance with the statistical weights of these levels.

200 to 250 Å in 0.02-Å steps. The dwell time was 1s/step and a total of 50 scans were accumulated. The fluorescent signal was divided by the signal from the photomultiplier tube (PMT) that monitored the intensity of the incident radiation. Because of the sodium salicylate coating on this PMT its response per unit photon flux was approximately constant over the narrow range of wavelengths studied [20]. Thus the ratio gives the relative cross section for producing the $3p(^4P^\circ)$ satellite state.

RESULTS AND DISCUSSION

The spectrum of the $3p(^4P^\circ)$ satellite is shown in Fig. 4. No direct transitions into the satellite continuum were observed and none would be expected in LS coupling because of violation of the spin selection rule. However, in jj coupling the transition is allowed. The lack of any measurable continuum implies jj coupling is weak in this case. The in direct processes, such as that given in Eq. (2), are clearly seen, showing that many different doubly excited configurations can autoionize into the $3p(^4P^\circ)$ continuum. The $3p(^2P^\circ)n(d,s)$ doubly excited Rydberg series is shown in Fig. 4(a) and clearly dominates the spectrum. The intensity of the 4d line of this series is about 2.5 times weaker than that of the 5d line. But this is because all terms above the 4d level can autoionize into each of the $^4P^\circ_{1/2,3/2,5/2}$ continua (see Fig. 1). In contrast, the 4d level lies below the $^4P^\circ_{1/2}$ threshold, and therefore cannot autoionize into its continuum, and it probably lies below the $^4P^\circ_{3/2}$ threshold. The $^4P^\circ_{3/2}$ threshold, determined from optical spectra [18,19], has an energy of 52.116 eV. The present measurement of the 4d energy level is 52.116±0.007 eV (237.90±0.03 Å). Codling, Madden, and Ederer [15] quote a value of 52.112±0.07 eV (237.92±0.03 Å). Thus the $^4P^\circ_{3/2}$ threshold lies within the error bars of the two measurements of the 4d energy level. However, based on the relative intensities of the 4d, 5d, and 6d lines we believe the 4d line lies just below the $^4P^\circ_{3/2}$ threshold. The relative intensities of these three lines in the present work are in the ratio of 1.89:4.6:1, respectively. Codling, Madden, and Ederer quote approximate ratios of 6:4:1 from their total absorption data. The difference between these ratios can be understood as follows. We can estimate the relative intensity of the fluorescent signals from each of the $^4P^\circ$ multiplets by us-

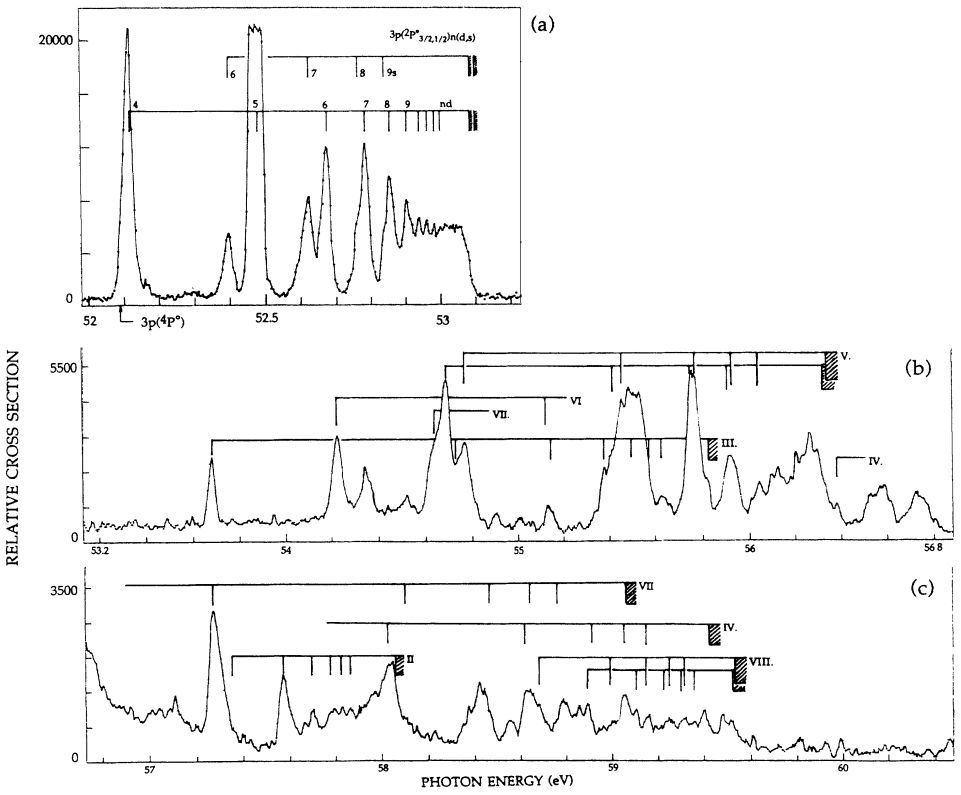

FIG. 4. The relative cross sections of the $3p(^4P^\circ)$ satellite state as a function of the incident photon energy. The threshold energy for the satellite is shown in (a) with the arrow at 52.088 eV. Because no continuum was observed, the zero level has been lowered for clarity. However, the intensity scales given in (a)–(c) can be used to get relative intensities between the various peaks. The energy levels of the various series are tabulated in the tables indicated by the Roman numerals.

TABLE I. The $(^3P)3p(^2P^\circ)n(s,d)$ Rydberg series. Values in parentheses reflect unresolved peaks.

	Present data				Codling, Madden, and Ederer
n	n^*	δ	λ (Å)	E (eV)	E (eV)
$4d$	3.748	0.252	237.90	52.116	52.112
5	4.734	0.266	236.26	52.478	52.478
6	5.739	0.261	235.39	52.672	52.658
7	6.699	0.301	234.90	52.782	
8	7.671	0.329	234.58	52.854	
9	8.657	0.343	234.36	52.903	
10	9.600	0.400	234.21	52.937	
11	10.430	0.570	234.11	52.960	
∞		average series limit		53.079	
$6s$	4.436	1.564	236.64	52.394	52.387
7	5.412	1.588	235.62	52.620	$(^1S)3s(^2S)3p$
8	6.46	1.54	(235.00)	(52.759)	52.737
9	7.39	1.61	(234.66)	(52.836)	52.827
∞		average series limit		53.081	
Spectroscopic series limits		$^2P^\circ_{3/2}$		53.077	
		$^2P^\circ_{1/2}$		53.093	

TABLE II. The $(^3P)4p(^2P^\circ)ns$ Rydberg series. Values in parentheses reflect unresolved peaks.

	Present data				Codling, Madden, and Ederer
n	n^*	δ	λ (Å)	E (eV)	assignment
$6s$	4.468	1.532	(216.21)	(57.344)	
7	5.485	1.515	215.37	57.568	$(^1S)3d(^2D)3p$
8	6.484	1.516	214.89	57.697	
9	7.484	1.516	214.59	57.777	
10	8.486	1.514	214.39	57.831	
11	9.484	1.516	214.25	57.869	
∞		average series limit		58.020	
Spectroscopic series limits		$^2P^\circ_{3/2}$		58.027	
		$^2P^\circ_{1/2}$		58.058	

TABLE III. The $(^1D)3p(^2P^\circ)ns$ Rydberg series. Values in parentheses reflect unresolved peaks.

	Present data				Codling Madden, and Ederer
n	n^*	δ	λ (Å)	E (eV)	E (eV)
$4s$	2.521	1.479	230.98	53.677	53.677
5	3.526	1.474	(226.56)	(54.725)	54.771
6	4.505	1.495	(224.82)	(55.148)	55.178
7	5.521	1.479	223.91	55.372	55.375
8	6.471	1.529	(223.42)	55.494	55.499
9	7.372	1.628	(223.12)	(55.568)	
10	8.344	1.656	222.90	55.623	
∞		average series limit		55.811	
Spectroscopic series limits		$^2P^\circ_{3/2}$		55.819	
		$^2P^\circ_{1/2}$		55.848	

TABLE IV. The $(^1S)3p(^2P^\circ)ns$ Rydberg series. Values in parentheses reflect unresolved peaks.

	Present data				Codling, Madden, and Ederer
n	n^*	δ	λ (Å)	E (eV)	assignment
$4s$	2.112	1.888	219.91	56.380	
5	3.119	1.881	(213.65)	(58.031)	(?)
6	4.103	1.897	(211.50)	(58.621)	(?)
7	5.122	1.878	(210.46)	(58.894)	
8	6.042	1.958	209.94	59.057	
9	6.974	2.026	209.61	59.150	
∞		average series limit		59.423	
Spectroscopic series limits		$^2P^\circ_{3/2}$		59.429	
		$^2P^\circ_{1/2}$		59.430	

ing the published spectroscopic data [18] corrected for the transmission of our interference filter. This results in relative intensities of 38%, 52%, and 10% of the signal originating from the 5/2, 3/2, and 1/2 multiplets, respectively. If the $4d$ level does not autoionize into the $^4P^\circ_{1/2,3/2}$ continua this represents a loss of 62% of the $4d$ intensity relative to the other levels. Correcting the $4d$ level for this loss yields relative intensities for the $4d$, $5d$, and $6d$ lines of 5:4.6:1, in reasonable agreement with Codling, Madden, and Ederer's estimate. Thus we conclude that the $4d$ level can only autoionize into the $^4P^\circ_{5/2}$ continuum.

Many of the peaks shown in Fig. 4 have been grouped into Rydberg series of doubly excited states, which terminate on the known excited states of Ne^+. The procedure used to identify a given series is given as follows: We start with the Rydberg formula

$$\nu_\infty - \nu_n = R/(n^*)^2, \quad \text{with } n^* = n + \delta , \tag{3}$$

where ν_∞ and ν_n are the wave numbers of the series limit and of the nth term of the series, respectively, n^* is the effective quantum number, and δ is the quantum defect. The wave numbers of suspected consecutive line pairs (n and $n+1$) were then subtracted in order to determine n^* and ν_∞. The average values of ν_∞ were compared to the known spectroscopic ionic states given by Persson [18]. This allowed identification of the Rydberg series. The effective quantum numbers were then redetermined using the spectroscopic value for ν_∞ and the observed values of ν_n. The Rydberg series, their energies, and effective quantum numbers are tabulated in Tables I–VIII and where possible are compared to the assignments given by Codling, Madden, and Ederer [15] and Wills *et al.* [13]. Our wavelength assignments agree within their respective

TABLE V. The $(^3P)3d(^2D_{5/2,3/2})np$ Rydberg series. Values in parentheses reflect unresolved peaks.

	Present data				Codling, Madden, and Ederer	Wills *et al.*
n	n^*	δ	λ (Å)	E (eV)	E (eV)	E (eV)
$4p_{(5/2)}$	2.892	1.109	226.72	54.686	54.676	54.68
5	3.890	1.110	(223.74)	(55.414)		55.40
6	4.874	1.126	(222.43)	(55.741)		55.755
7	5.856	1.144	(221.73)	(55.917)		
∞		average series limit		56.310		
Spectroscopic series limit		$^2D_{5/2}$		56.313		
$4p_{(3/2)}$	2.939	1.061	226.40	54.763		
5	3.921	1.079	223.58	55.454		
6	4.906	1.095	(222.30)	(55.773)		
7	5.819	1.181	(221.65)	(55.937)		
8	6.783	1.217	221.23	56.043		
∞		average series limit		56.325		
Spectroscopic series limit		$^2D_{3/2}$	56.339			

TABLE VI. The $(^3P)3d(^4D)np$ Rydberg series.

	Present data				Codling, Madden, and Ederer
n	n^*	δ	λ (Å)	E (eV)	assignment
$4p$	2.637	1.363	228.66	54.222	$(^1D)3d(^2D3)p$
5	3.600	1.400	224.90	55.129	
∞		average series limit		59.145	
Spectroscopic series limits		$^2D_{7/2,5/2}$		59.178	

TABLE VII. The $(^3P)4d(^2D)np$ Rydberg series. Values in parentheses reflect unresolved peaks.

	Present data				Codling, Madden, and Ederer
n	n^*	δ	λ (Å)	E (eV)	assignment
$3p$	1.754	1.246	226.94	54.633	$(^1S)3p(^2P)4s$
4	2.762	1.238	(216.49)	(57.270)	
5	3.772	1.228	213.41	58.097	(?)
6	4.793	1.207	(212.08)	(58.461)	
7	5.771	1.229	(211.41)	(58.646)	(?)
8	6.815	1.185	(211.00)	(58.760)	
∞		average series limit		59.060	
Spectroscopic series limits		$^2D_{5/2}$		59.046	
		$^2D_{3/2}$		59.061	

TABLE VIII. The $(^1D)3d(^2D)n(p,f)$ Rydberg series. Values in parentheses reflect unresolved peaks.

	Present data				Codling, Madden, and Ederer	Wills *et al.*
n	n^*	δ	λ (Å)	E (eV)	E (eV)	E (eV)
$4f$	3.988	0.012	211.29	56.680		
5	4.981	0.019	(210.19)	(58.987)		
6	5.943	0.057	209.61	59.150		
7	6.929	0.072	209.25	59.252		
8	7.845	0.155	(209.03)	(59.314)		
∞		average series limit		59.527		
$3p$	1.600	1.400	228.66	54.222	54.217	54.21
6	4.608	1.392	210.52	58.894		58.905
7	5.624	1.376	209.77	59.105		59.105
8	6.607	1.393	209.35	59.223		
9	7.746	1.254	(209.05)	(59.308)		
10	8.733	1.267	208.88	59.357		
∞		average series limit		59.541		
Spectroscopic series limit		$^2D_{(5/2)}$		59.534		
		$^2D_{(3/2)}$		59.536		

error bars, in practically every case with those quoted by Codling, Madden, and Ederer. However, in some cases we disagree with a particular configuration assignment and these are noted in the tables. Furthermore, we find that some of their broad lines are actually composites of several lines. In these cases we have made approximate deconvolutions to determine the underlying structure. When peaks are not resolved the tabulated data are placed in parentheses.

The selection of the appropriate angular momentum for the Rydberg electron was based on the value of δ, the quantum defect for a given series. We found that the various values of δ fell naturally into four groups. On the basis that we expect δ to decrease in value as the electron orbital angular momentum increases we have assigned a given nl to each group as follows:

$$\delta(ns)\sim 1.5-1.9,\quad \delta(np)\sim 1.0-1.4,$$
$$\delta(nd)\sim 0.2-0.3,\quad \delta(nf)\sim 0\ .$$

The photoelectron studies of Willis *et al.* [13] have shown that individual doubly excited states will autoionize into several different satellite continua with varying degrees of intensity. In order to identify any systematic trends we have listed all the doubly excited Rydberg series that we have identified, which autoionize into the $3p(^4P^\circ)$ satellite. Namely,

$$\left.\begin{array}{l}(^3P)3p(^2P^\circ)n(d,s)^{1,3}P_1^\circ\\ (^3P)4p(^2P^\circ)n(d,s)^{1,3}P_1^\circ\\ (^1D)3p(^2P^\circ)n(d,s)^{1,3}P_1^\circ\\ (^1S)3p(^2P^\circ)n(d,s)^{1,3}P_1^\circ\end{array}\right\}\rightarrow 2s^2 2p^4(^3P)3p(^4P^\circ)+e^-\ .$$

$$\left.\begin{array}{l}(^3P)3d(^2D)n(p,f)^{1,3}P_1^\circ\\ (^3P)4d(^2D)n(p,f)^{1,3}P_1^\circ\\ (^1D)3d(^2D)n(p,f)^{1,3}P_1^\circ\\ (^3P)3d(^4D)n(p,f)^{1,3}P_1^\circ\end{array}\right\}$$

With pure LS coupling an optical transition from the ground $^1S_0$ into a $^1P_1^\circ$ final state is allowed. However, no autoionization can occur to the $^4P_1^\circ$ ionic state. The fact that autoionization does occur is evidence that the initial absorption process did not proceed via pure LS coupling. In fact, the transition requires the two-electron excitation configurations to interact with each other causing a mixture of the singlet and triplet states. Thus we have used the notation $^{1,3}P_1^\circ$ to describe the final-state configuration. With this mixing we would expect autoionization of the $(^3P)3p(^2P)n(s,d)^{1,3}P_1^\circ$ series to be strong. Other transitions that require a core change from a ^3P to a ^1D or ^1S state or require a change in the angular momentum of the non-Rydberg-electron should be much weaker, as we have observed. We have identified only one series that requires both a core change and a change in the orbital angular momentum of the non-Rydberg-electron, namely, the $(^1D)3d(^2D)n(p,f)$ series (see Table VIII). This is certainly one of the weaker series that we observe.

No quantitative measurement of the relative intensities of the various series can be made with the present resolution. However, qualitatively, the greater the number of electrons that must readjust, the weaker the intensity of autoionization. This statement must be tempered, of course, because the initial strength of the doubly excited neutral states will also affect the apparent intensity of autoionization.

A study of the autoionization of doubly excited neutral states in the rare gases can yield direct information about the breakdown of LS coupling in the initial absorption process. As we have seen in the above analysis the observation of autoionization into a quartet state of a satellite is a way of monitoring this breakdown. Another example is given by observing the autoionizing structure in the $(^3P)3s(^2P)$ and $(^3P)3s(^4P)$ satellite states of Ne as reported by Schartner *et al.* [12] and Wills *et al.* [13]. They observed that the doubly excited neutral state $(^1D)3s(^2D)4p(^1P_1)$ autoionized only into the $(^3P)3s(^2P)$ satellite and not into the $(^3P)3s(^4P)$ satellite. This implies that LS coupling is the dominant process in producing the initial doubly excited neutral state, thus leaving it in a $^1P_1$ final state. On the other hand, the identical transition in Ar, namely, the $(^1D)4s(^2D)5p(^1P_1)$ state does autoionize strongly into the $(^3P)4s(^4P)$ satellite [6–8]. This indicates a breakdown of LS coupling and a mixing of the singlet and triplet states during the initial absorption process leaving the doubly excited Ar in a $^{1,3}P_1$ final state. The breakdown in LS coupling is expected to increase as the atomic number of the atom increases.

ACKNOWLEDGMENTS

It is a pleasure to thank Professor Starace and Dr. Pan for many stimulating discussions, and Dr. Madden and Dr. Ederer for making available detailed photographs of their doubly excited spectra of neon. This material is based upon work supported by the National Science Foundation (NSF) under Grant No. PHY-9017248. We also wish to acknowledge the help of the personnel at the Stoughton Synchrotron Radiation Center, which is supported by NSF Grant No. 88-21625.

[1] P. R. Woodruff and J.A.R. Samson, Phys. Rev. Lett. **45**, 110 (1980).

[2] P. R. Woodruff and J.A.R. Samson, Phys. Rev. A **25**, 848 (1982).

[3] D. W. Lindle, T. A. Ferret, U. Becker, P. H. Korbin, C. M. Truesdale, H. G. Kerkhoff, and D. Shirley, Phys. Rev. A **31**, 714 (1985).

[4] U. Becker, R. Hölzel, H. G. Kerkhoff, B. Langer, D. Szostak, and R. Wehlitz, Phys. Rev. Lett. **56**, 1120 (1986).

[5] U. Becker, B. Langer, H. G. Kerkhoff, M. Kupsch, D. Szostak, and R. Wehlitz, Phys. Rev. Lett. **60**, 1490 (1988).

[6] K.-H. Schartner, B. Möbus, H. Schmoranzer, and M.

Wildberger, Phys. Rev. Lett. **61**, 2744 (1988).
[7] A. A. Wills, A. A. Cafolla, F. J. Currell, J. Comer, A. Svensson, and M. A. MacDonald, J. Phys. B **22**, 3217 (1989).
[8] R. I. Hall, L. Avaldi, G. Dawber, P. M. Rutter, M. A. MacDonald, and G. C. King, J. Phys. B **22**, 3205 (1989).
[9] M. Zubeck, G. C. King, P. M. Rutter, and F. H. Read, J. Phys. B **22**, 3411 (1989).
[10] J.A.R. Samson, E. M. Lee, and Y. Chung, Phys. Scr. **41**, 850 (1990).
[11] K.-H. Schartner, P. Lenz, B. Möbus, and B. Magel, Phys. Scr. **41**, 853 (1990).
[12] K.-H. Schartner, B. Magel, B. Möbus, H. Schmoranzer, and M. Wildberger, J. Phys. B **23**, L527 (1990).
[13] A. A. Wills, A. A. Cafolla, A. Svensson, and J. Comer, J. Phys. B **23**, 2013 (1990).
[14] A. A. Wills, A. A. Cafolla, and J. Comer, J. Phys. B **23**, 2029 (1990).
[15] K. Codling, R. P. Madden, and D. L. Ederer, Phys. Rev. **155**, 26 (1967).
[16] W. Wijesundera and H. P. Kelly, Phys. Rev. A **36**, 4539 (1987).
[17] W. Wijesundera and H. P. Kelly, Phys. Rev. A **39**, 634 (1989).
[18] W. Persson, Phys. Scr. **3**, 133 (1971).
[19] C. E. Moore, *Ionization Potentials and Ionization Limits Derived from the Analyses of Optical Spectra,* Natl. Bur. Stand. Ref. Data Ser. Natl. Bur. Stand. (U.S.) Circ. No. 34 (U.S. GPO, Washington, D. C., 1970).
[20] J.A.R. Samson and G. N. Haddad, J. Opt. Soc. Am. **64**, 1346 (1974).